Supplement of Clim. Past, 22, 1–16, 2026
https://doi.org/10.5194/cp-22-1-2026-supplement

Climate of the Past Open Access EGU

Supplement of

The relative impacts of tropical Pacific teleconnections and local insolation on mid-Holocene precipitations over tropical South America

Minn Lin Wong and Xianfeng Wang

Correspondence to: Minn Lin Wong (minnlin001@e.ntu.edu.sg)

S1. Method details for MidH ECHAM4.6 experiment

In order to force a mid-Holocene climatological SST over the tropical Pacific in the MidH experiment, the ECHAM4.6 is forced with 41-years of modern SSTs, however, the tropical Pacific region (160–275°E; 20°N–20°S) is prescribed with the climatological SST based on the ensemble mean of mid-Holocene simulations from PMIP4 (Fig. S1). First, the year-to-year variability within the tropical Pacific box is suppressed by imposing the 41-year (1979–2019) climatology in the box. This removes the modern-day ENSO variability (as was done in the NoENSO experiment). Next, to shift the climatological SSTs to the mid-Holocene state, we derive the difference in the climatological cycle between the PMIP4 'mid-Holocene' ensemble and CMIP6 'Historical' simulations. The specific models used are shown in Table S1. The difference in the mean climatological annual cycle is then added to the tropical Pacific SSTs.

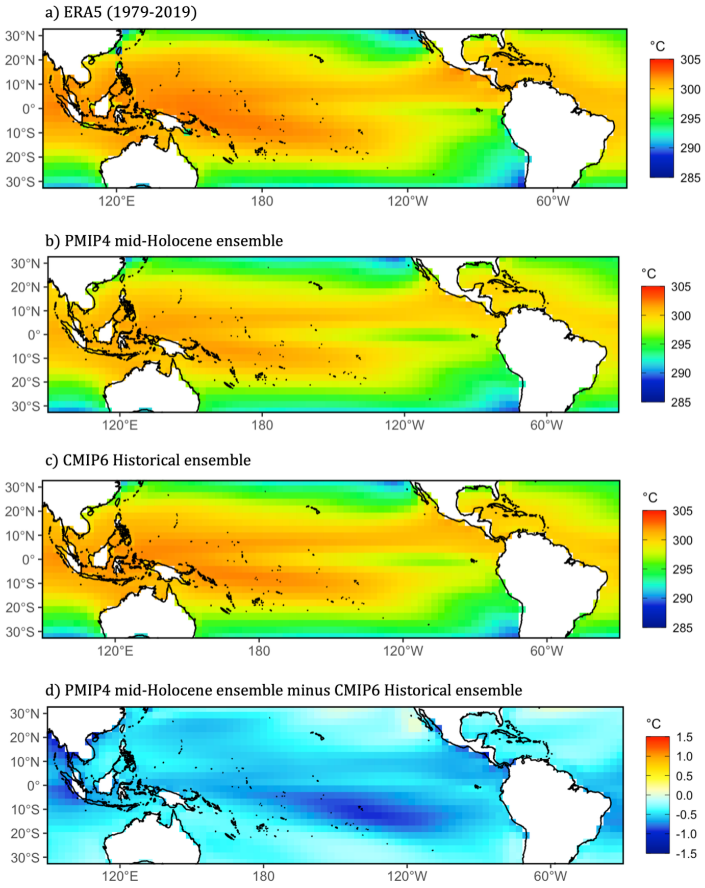

Figure S1: Annual mean climatological SST from (a) ERA5 (1979–2019), (b) PMIP4 mid-Holocene ensemble annual mean SSTs, (c) CMIP6 Historical scenario, and (d) the difference in the ensemble annual mean SSTs, mid-Holocene minus historical (panel b minus panel c).

Table S1: Models used in the calculation of the PMIP4 mid-Holocene ensemble and CMIP6 Historical ensemble (data accessed from https://aims2.llnl.gov/search).

Model
ACCESS-ESM1-5
AWI-ESM-1-1-LR
CESM2
EC-Earth3
FGOALS-f3-L
FGOALS-g3
GISS-E2-1-G
INM-CM4-8
IPSL-CM6A-LR
MPI-ESM1-2-LR
MRI-ESM2-0
NESM3
NorESM2-LM
NorESM1-F*

* Only available for the mid-Holocene scenario.

S2. $\delta^{18}O$ proxy records in tropical South America

Most speleothem $\delta^{18}O$ records in South America are catalogued in the Speleothem Isotopes Synthesis and Analysis (SISAL v2) database (Comas-Bru et al., 2020; Deininger et al., 2019). Speleothem $\delta^{18}O$ in the SISAL_V2 is presented with respect to the Vienna Pee Dee Belemnite standard (VPDB) and the values are dependent on the mineralogy of the samples, which can differ between aragonite and calcite. Therefore, we convert speleothem $\delta^{18}O$ values to their dripwater equivalents relative to the Vienna Standard Mean Ocean Water (VSMOW) using a fractionation factor for sample mineralogy (either aragonite or calcite), and the cave site temperatures that are specified by their respective authors. Samples which have unknown, or a mixed mineralogy are excluded from this analysis. The $\delta^{18}O$ proxy records that fulfil the above requirements are shown in Table S2, along with other $\delta^{18}O$ records from lake carbonates and ice cores. They are relatively evenly spread across the continent and can provide an adequate depiction of broad spatial patterns.

In Table S2, the mid-Holocene is defined as 5000–7000 BP, the pre-industrial is defined as 850–1850 CE, and the historical period is defined as 1850–2014 CE. The interpretations of mid-Holocene hydroclimate conditions ('dry', 'similar', and 'wet') are taken directly from the respective original publications of each record, following the approach of Prado et al. (2013), such that no additional interpretation is imposed in this study.

There are minor differences in $\delta^{18}O$ values between the historical (1850–2014 CE) and pre-industrial (850–1850 CE) intervals as multidecadal modes of variability in both the Pacific and Atlantic basins have been shown to influence $\delta^{18}O$ in precipitation over South America from the pre-industrial onwards (Orrison et al., 2022). Nevertheless, these differences are minor compared to the larger mid-Holocene shifts, indicating that the mid-Holocene interpretation remains robust despite potential modulation by decadal-to-multidecadal variability since the pre-industrial. Furthermore, the amount of tropical warming from 850 CE to present is ≤ 1°C, or in terms of $\delta^{18}O$, less than −0.24‰/°C (Kim and O'Neil, 1997). Comparing speleothem $\delta^{18}O$ in columns 8 to 11 of Table S2 confirms our expectation that $\delta^{18}O$ over the pre-industrial period is indeed very similar to that over the historical period. Only one record, the Huascaran ice core (which contains a single sample within the historical period), shows a reversal in the direction of change, and several records have limited sample coverage during the historical interval. Hence, to compare the observed and simulated changes in the $\delta^{18}O$ of precipitation since the mid-Holocene, we use the observed $\delta^{18}O$ over the pre-industrial period (850–1850 CE) in place of the $\delta^{18}O$ over the historical period (1850–2014 CE) to take advantage of the much larger sample size available when using the pre-industrial values and to enable us to include the ice core records in our comparison of simulated and observed $\delta^{18}O$.

Table S2: $\delta^{18}O$ records used in this study, and the inferred difference in mid-Holocene precipitation relative to modern day (sixth column). The last four columns show the average $\delta^{18}O$ values from each proxy record for the mid-Holocene and pre-industrial timeframes, the difference between mid-Holocene and pre-industrial, and in the final column, the difference between mid-Holocene and the historical period. The number of sample points used for the historical period is shown in brackets. Locations of each site are shown in Fig. S2.

Site No.	Site name	Lon	Lat	Type of archive	Mid-Holocene condition	Samples	**MH** $\delta^{18}O$	**PI** $\delta^{18}O$	**MH-PI** $\delta^{18}O$	**MH-Hist** $\delta^{18}O$
1	Botuverá Cave[1]	-49.02	-27.13	Speleothem	Dry	1055	-2.82	-5.71	2.89	2.92 (584)
2	Jaraguá Cave[2]	-56.35	-21.00	Speleothem	Dry	205	-3.55	-4.83	1.28	1.28 (33)
3	Huagapo Cave[3]	-75.79	-11.47	Speleothem	Dry	209	-12.40	-13.37	0.97	0.81 (32)
4	Paraíso Cave[4]	-55.45	-4.07	Speleothem	Wet	119	-8.01	-5.71	-2.30	-2.24 (26)
5	Rio Grande do Norte[5]	-37.44	-5.60	Speleothem	Wet	41	-6.21	-2.56	-3.65	-3.91 (2)
6	Paixão Cave[6]	-41.02	-12.63	Speleothem	Wet					
7	Angelica Cave[7]	-46.23	-13.40	Speleothem	Similar	46	-2.97	-2.65	-0.32	NA (0)
8	Lapa Grade Cave[8]	-44.36	-14.42	Speleothem	Similar					
9	Shatuca Cave[9]	-77.90	-5.70	Speleothem	Dry	36	-5.85	-5.89	0.40	0.32 (16)
10	Cueva del Tigre Perdido[10]	-77.30	-5.94	Speleothem	Dry	34	-7.06	-7.09	0.58	0.63 (3)
11	Santana Cave[11]	-48.72	-24.53	Speleothem	Dry					
12	El Condor Cave[12]	-77.18	-5.56	Speleothem	Dry					
13	Cueva del Diamante[12]	-77.30	-5.44	Speleothem	Dry					
14	Huascaran[13]	-77.50	-9.00	Ice core	Dry	10	-17.61	-18.52	0.91	-0.23 (1)
15	Sajama[14]	-68.53	-18.06	Ice core	Dry	10	-16.41	-16.47	0.06	1.02 (1)
16	Laguna Pumacocha[15]	-76.06	-10.70	Lake Carbonate	Dry	541	18.64	16.86	1.78	1.37 (157)
17	Lake Junin[16]	-76.11	-11.03	Lake Carbonate	Dry					

[1]Wang et al. (2017)
[2]Novello et al. (2017)
[3]Kanner et al. (2013)
[4]Wang et al. (2017)

[5]Cruz et al., (2009)
[6]Barreto and Cruz (2010)
[7]Wong et al. (2021)
[8]Strikis et al. (2011)
[9]Bustamante et al. (2016)
[10]Breukelen et al. (2008)
[11]Cruz et al. (2006)
[12]Cheng et al., (2013)
[13]Thompson et al. (1995)
[14]Reese et al. (2013)
[15]Bird et al., (2011)
[16]Seltzer et al. (2000)

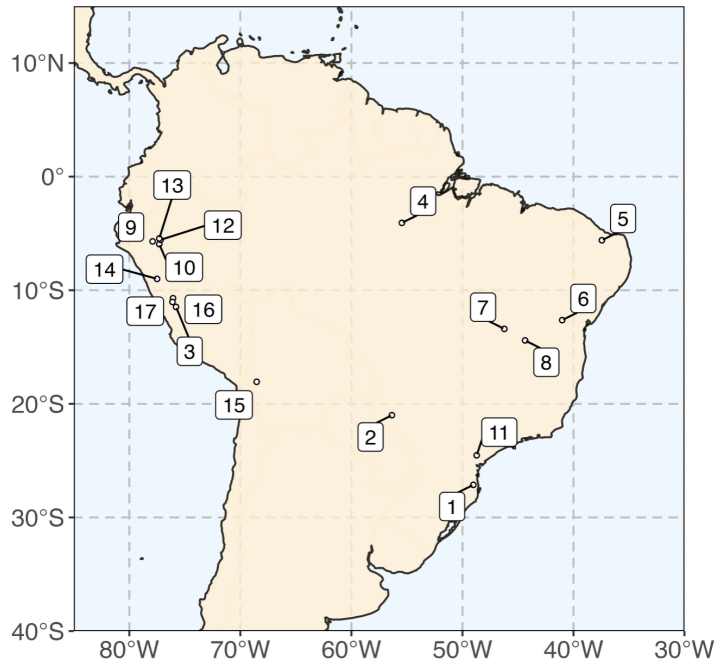

Figure S2: Location of each of the paleorecords listed in Table S2. Numbers refer to the site number in the first column of Table S2.

S3. Performance of ECHAM4.6 model

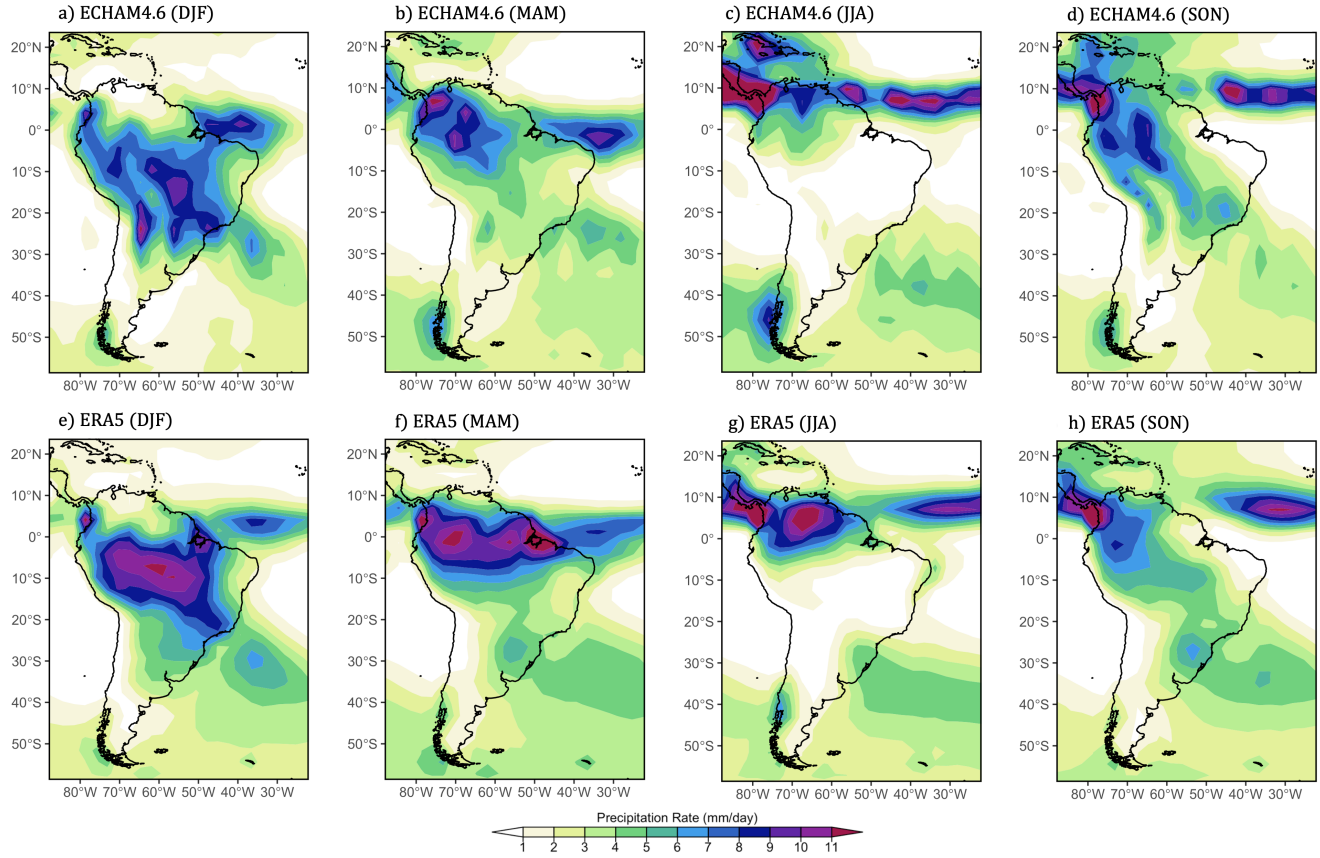

Figure S3: Seasonal precipitation rates over South America (a–d) simulated by ECHAM4.6 with prescribed SSTs over 40-years from 1980–2019 and (e–h) from ERA5 reanalysis (Hersbach et al., 2020) over the same 40-year period. Austral summer (DJF), spring (MAM), winter (JJA) and autumn (SON) climatology is shown in (a/e), (b/f), (c/g) and (d/h) respectively.

S4. ECHAM4.6 $\delta^{18}O$ comparison

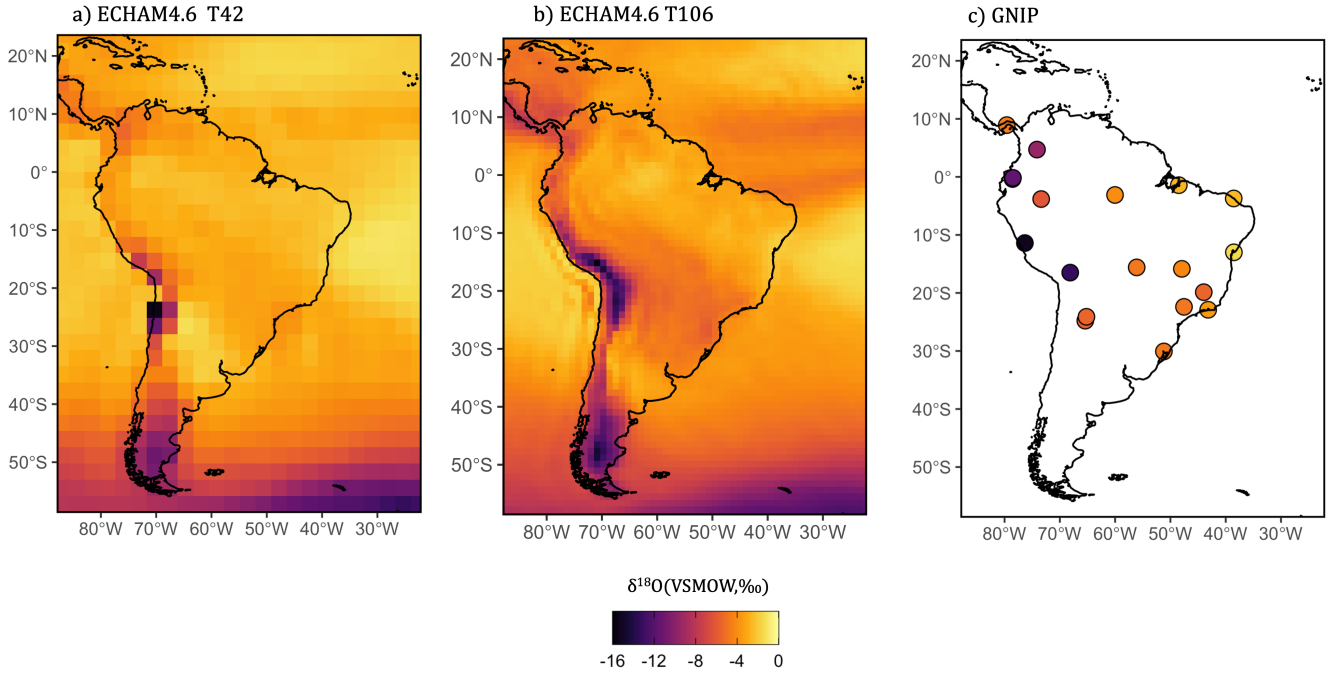

Figure S4: Comparisons of modern day $\delta^{18}O_p$ simulated by ECHAM4.6 at (a) T42 resolution in the current study, and (b) T106 resolution by X. Liu (2022, personal communication), showing a larger inland $\delta^{18}O$ gradient when the model is run with a higher resolution. (c) Measured $\delta^{18}O_p$ from the Global Network of Isotopes in Precipitation (GNIP) stations (IAEA/WMO, 2021).

S5. ECHAM4.6 simulation of El Niño/La Niña impact on South America

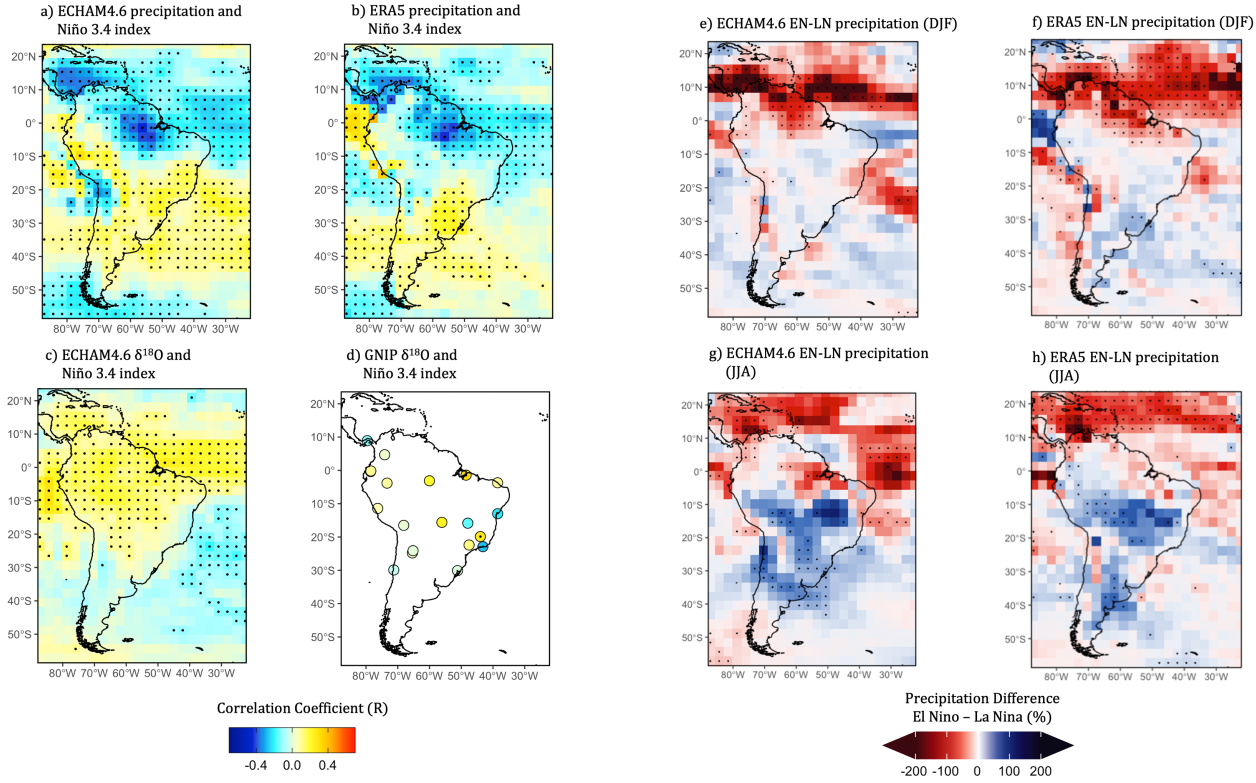

Figure S5: Modern-day ENSO-related anomalies in precipitation (a) simulated by ECHAM4.6 and (b) from ERA5 reanalyses data, found by correlating monthly values of these fields with Niño3.4. The modern-day ENSO-related anomalies are found from the Control simulation. (c) and (d) as in (a) and (b), but for the $\delta^{18}O$ of precipitation. Panel (d) shows the correlations of precipitation $\delta^{18}O$ from GNIP stations with Nino 3.4 index. The difference in precipitation (percentage), calculated as the anomaly between El Niño and La Niña years and normalized by the El Niño composite precipitation, is shown for DJF in (e) ECHAM4.6 Control simulation and (f) ERA5 Reanalysis data; and for JJA in (g) the ECHAM4.6 simulation and (h) ERA5 Reanalysis data. Stippled regions are where the correlation or precipitation difference is significant at a 95% confidence level.

S6. Differences in mid-Holocene simulation with coupled slab ocean model

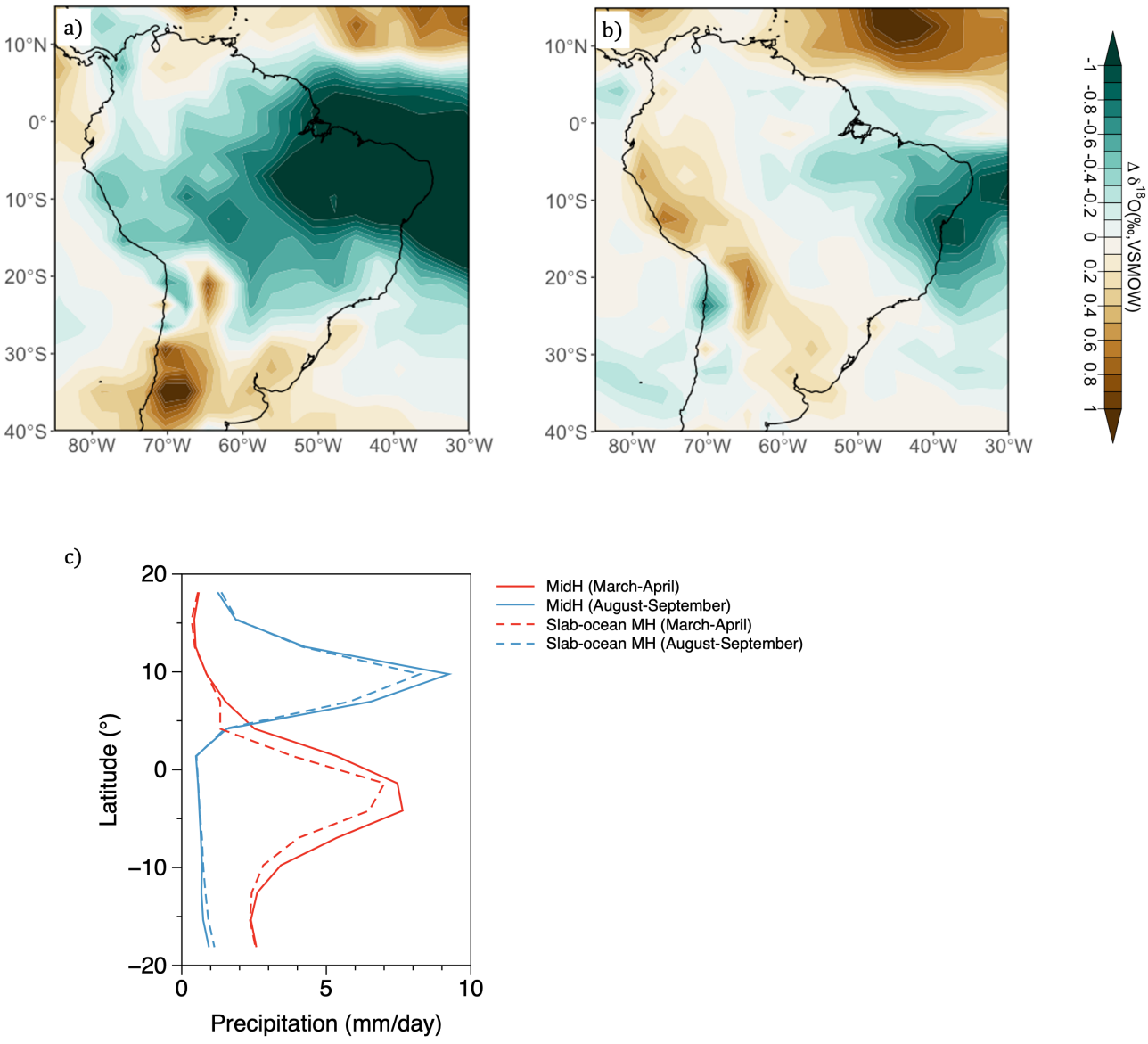

Figure S6: Mid-Holocene minus modern day $\delta^{18}O_p$ simulated by ECHAM4.6 (a) from the experiments in this study using prescribed SSTs (MidH minus Control), and (b) coupled to a slab ocean model (Wong et al., 2023). The simulated ITCZ strength is shown in (c), showing the averaged (between 60°W and 0°) precipitation for March–April (in red) and August-September (in blue) for the mid-Holocene prescribed SST experiment (MidH) in the solid line, and for the mid-Holocene scenario using the same model coupled to a slab-ocean model in dashed line (Slab-ocean MH).

References

Barreto,E. A. S. and Cruz, F. W.: Precipitation reconstruction in Chapada Diamantina (BA) during the Late Quaternary through isotopic records (O e C) on stalagmites, UNIVERSIDADE DE SÃO PAULO, INSTITUTO DE GEOCIÊNCIAS, 2010.

Bird, B. W., Abbott, M. B., Vuille, M., Rodbell, D. T., Stansell, N. D., and Rosenmeier, M. F.: A 2,300-year-long annually resolved record of the South American summer monsoon from the Peruvian Andes, Proceedings of the National Academy of Sciences, 108, 8583–8588, https://doi.org/10.1073/pnas.1003719108, 2011.

van Breukelen, M. R., Vonhof, H. B., Hellstrom, J. C., Wester, W. C. G., and Kroon, D.: Fossil dripwater in stalagmites reveals Holocene temperature and rainfall variation in Amazonia, Earth and Planetary Science Letters, 275, 54–60, https://doi.org/10.1016/j.epsl.2008.07.060, 2008.

Bustamante, M. G., Cruz, F. W., Vuille, M., Apaéstegui, J., Strikis, N., Panizo, G., Novello, F. V., Deininger, M., Sifeddine, A., Cheng, H., Moquet, J. S., Guyot, J. L., Santos, R. V., Segura, H., and Edwards, R. L.: Holocene changes in monsoon precipitation in the Andes of NE Peru based on δ18O speleothem records, Quaternary Science Reviews, 146, 274–287, https://doi.org/10.1016/j.quascirev.2016.05.023, 2016.

Cheng, H., Sinha, A., Cruz, F. W., Wang, X., Edwards, R. L., d'Horta, F. M., Ribas, C. C., Vuille, M., Stott, L. D., and Auler, A. S.: Climate change patterns in Amazonia and biodiversity, Nat Commun, 4, 1411, https://doi.org/10.1038/ncomms2415, 2013.

Comas-Bru, L., Rehfeld, K., Roesch, C., Amirnezhad-Mozhdehi, S., Harrison, S. P., Atsawawaranunt, K., Ahmad, S. M., Brahim, Y. A., Baker, A., Bosomworth, M., Breitenbach, S. F. M., Burstyn, Y., Columbu, A., Deininger, M., Demény, A., Dixon, B., Fohlmeister, J., Hatvani, I. G., Hu, J., Kaushal, N., Kern, Z., Labuhn, I., Lechleitner, F. A., Lorrey, A., Martrat, B., Novello, V. F., Oster, J., Pérez-Mejías, C., Scholz, D., Scroxton, N., Sinha, N., Ward, B. M., Warken, S., Zhang, H., and members, S. W. G.: SISALv2: a comprehensive speleothem isotope database with multiple age–depth models, Earth System Science Data, 12, 2579–2606, https://doi.org/10.5194/essd-12-2579-2020, 2020.

Cruz, F. W., Burns, S. J., Karmann, I., Sharp, W. D., and Vuille, M.: Reconstruction of regional atmospheric circulation features during the late Pleistocene in subtropical Brazil from oxygen isotope composition of speleothems, Earth and Planetary Science Letters, 248, 495–507, https://doi.org/10.1016/j.epsl.2006.06.019, 2006.

Cruz, F. W., Vuille, M., Burns, S. J., Wang, X., Cheng, H., Werner, M., Lawrence Edwards, R., Karmann, I., Auler, A. S., and Nguyen, H.: Orbitally driven east–west antiphasing of South American precipitation, Nature Geoscience, 2, 210–214, https://doi.org/10.1038/ngeo444, 2009.

Deininger, M., Ward, B. M., Novello, V. F., and Cruz, F. W.: Late Quaternary Variations in the South American Monsoon System as Inferred by Speleothems—New Perspectives Using the SISAL Database, Quaternary, 2, https://doi.org/10.3390/quat2010006, 2019.

Hersbach, H., Bell, B., Berrisford, P., Hirahara, S., Horányi, A., Muñoz-Sabater, J., Nicolas, J., Peubey, C., Radu, R., Schepers, D., Simmons, A., Soci, C., Abdalla, S., Abellan, X., Balsamo, G., Bechtold, P., Biavati, G., Bidlot, J., Bonavita, M., De Chiara, G., Dahlgren, P., Dee, D., Diamantakis, M., Dragani, R., Flemming, J., Forbes, R., Fuentes, M., Geer, A., Haimberger, L., Healy, S., Hogan, R. J., Hólm, E., Janisková, M., Keeley, S., Laloyaux, P., Lopez, P., Lupu, C., Radnoti, G., de Rosnay, P., Rozum, I., Vamborg, F., Villaume, S., and Thépaut, J.-N.: The ERA5 global reanalysis, Quarterly Journal of the Royal Meteorological Society, 146, 1999–2049, https://doi.org/10.1002/qj.3803, 2020.

Kanner, L. C., Burns, S. J., Cheng, H., Edwards, R. L., and Vuille, M.: High-resolution variability of the South American summer monsoon over the last seven millennia: insights from a speleothem record from the central Peruvian Andes, Quaternary Science Reviews, 75, 1–10, https://doi.org/10.1016/j.quascirev.2013.05.008, 2013.

Kim, S.-T. and O'Neil, J. R.: Equilibrium and nonequilibrium oxygen isotope effects in synthetic carbonates, Geochimica et Cosmochimica Acta, 61, 3461–3475, https://doi.org/10.1016/S0016-7037(97)00169-5, 1997.

Novello, V. F., Cruz, F. W., Vuille, M., Stríkis, N. M., Edwards, R. L., Cheng, H., Emerick, S., de Paula, M. S., Li, X., Barreto, E. de S., Karmann, I., and Santos, R. V.: A high-resolution history of the South American Monsoon from Last Glacial Maximum to the Holocene, Scientific Reports, 7, 44267, https://doi.org/10.1038/srep44267, 2017.

Orrison, R., Vuille, M., Smerdon, J. E., Apaéstegui, J., Azevedo, V., Campos, J. L. P. S., Cruz, F. W., Della Libera, M. E., and Stríkis, N. M.: South American Summer Monsoon variability over the last millennium in paleoclimate records and isotope-enabled climate models, Climate of the Past, 18, 2045–2062, https://doi.org/10.5194/cp-18-2045-2022, 2022.

Prado, L. F., Wainer, I., Chiessi, C. M., Ledru, M.-P., and Turcq, B.: A mid-Holocene climate reconstruction for eastern South America, Climate of the Past, 9, 2117–2133, https://doi.org/10.5194/cp-9-2117-2013, 2013.

Reese, C. A., Liu, K. B., and Thompson, L. G.: An ice-core pollen record showing vegetation response to Late-glacial and Holocene climate changes at Nevado Sajama, Bolivia, Annals of Glaciology, 54, 183–190, https://doi.org/10.3189/2013AoG63A375, 2013.

Seltzer, G., Rodbell, D., and Burns, S.: Isotopic evidence for late Quaternary climatic change in tropical South America, Geology, 28, 35–38, https://doi.org/10.1130/0091-7613(2000)28%253C35:IEFLQC%253E2.0.CO;2, 2000.

Strikis, N., Cruz, F., Cheng, H., Karmann, I., Edwards, R., Vuille, M., Wang, X., de Paula, M., Novello, V., and Auler, A.: Abrupt variations in South American monsoon rainfall during the Holocene based on a speleothem record from central-eastern Brazil, Geology, 39, https://doi.org/10.1130/G32098.1, 2011.

Thompson, L. G., Mosley-Thompson, E., Davis, M. E., Lin, P.-N., Henderson, K. A., Cole-Dai, J., Bolzan, J. F., and Liu, K. -b.: Late Glacial Stage and Holocene Tropical Ice Core Records from Huascarán, Peru, Science, 269, 46–50, https://doi.org/10.1126/science.269.5220.46, 1995.

Wang, X., Edwards, R. L., Auler, A. S., Cheng, H., Kong, X., Wang, Y., Cruz, F. W., Dorale, J. A., and Chiang, H. W.: Hydroclimate changes across the Amazon lowlands over the past 45,000 years, Nature, 541, 204–207, https://doi.org/10.1038/nature20787, 2017.

Wong, M. L., Wang, X., Latrubesse, E. M., He, S., and Bayer, M.: Variations in the South Atlantic Convergence Zone over the mid-to-late Holocene inferred from speleothem δ18O in central Brazil, Quaternary Science Reviews, 270, 107178, https://doi.org/10.1016/j.quascirev.2021.107178, 2021.

Wong, M. L., Battisti, D. S., Liu, X., Ding, Q., and Wang, X.: A North–South Dipole Response of the South Atlantic Convergence Zone During the Mid-Holocene, Geophysical Research Letters, 50, e2023GL105130, https://doi.org/10.1029/2023GL105130, 2023.